Crystallization and transformation behavior of triacylglycerol binary mixtures forming molecular compounds of POP/OPO, POP/*rac*-PPO, and POP/*sn*-PPO

Laura Bayés-García,† Koji Fukao,‡ Takashi Konishi,¶ Kiyotaka Sato,§ and Ken Taguchi[*, ‖]

†Departament de Mineralogia, Petrologia i Geologia Aplicada, Universitat de Barcelona, Barcelona, Spain

‡Department of Physics, Ritsumeikan University, Kusatsu, Shiga 525-8577, Japan

¶Graduate School of Human and Environmental Studies, Kyoto University, Sakyo-ku, Kyoto 606-8501, Japan

§Faculty of Applied Biological Science, Hiroshima University, Higashi-Hiroshima 739-8528, Japan

‖Graduate School of Advanced Science and Engineering, Hiroshima University, Higashi-Hiroshima 739-8521, Japan

Email: ktaguchi@hiroshima-u.ac.jp

KEYWORDS. Triacylglycerol, Binary mixture, Polymorphism, Molecular compound formation, Crystallization kinetics

ABSTRACT

Fat-based soft materials generally contain different triacylglycerol (TAG) species; hence, TAG mixtures' phase behaviors determine their important physical properties. TAG binary mixtures typically exhibit eutectic, monotectic, solid solution, and molecular compound (MC) forming phases; among them, the molecular interactions and the crystallization kinetics controlling the formation processes of MC-phases remain unexplored. We used thermal analysis, X-ray diffraction, and optical microscopy to examine the crystallization and transformation kinetics of the three MC-forming 1:1 binary TAG mixtures of 1,3-dipalmitoyl-2-oleoyl glycerol (POP)/1,3-dipalmitoyl-2-oleoyl glycerol (OPO), POP/1,2-dipalmitoyl-2-oleoyl-*rac*-glycerol (*rac*-PPO), and POP/1,2- dipalmitoyl-3-oleoyl-*sn*-glycerol (*sn*-PPO). In the POP/OPO mixture, the $MC_{POP/OPO}$ crystals of the most stable β form with double chain length stacking (β-2L) were crystallized by simple cooling treatments. In the POP/*rac*-PPO mixture, the β-2L form of $MC_{POP/rac\text{-}PPO}$ was crystallized by only cooling at 0.1 °C/min, while metastable β'-2L formed at the cooling rates of 0.5 °C/min and 2.0 °C/min; then β'-2L melted and partially transformed into the β form during the heating processes. The POP/*sn*-PPO mixture showed different and significantly intricate polymorphic behavior. First, a single component of *sn*-PPO crystallized in β' with triple chain length stacking (β'-3L) during cooling. This was followed by the crystallization of POP and $MC_{POP/sn\text{-}PPO}$ of the β'-2L forms at slow cooling rates of 0.1 °C/min and 0.5 °C/min, and the α-2L forms at 2.0 °C/min. During heating, the metastable β' or α forms melted and $MC_{POP/sn\text{-}PPO}$ transformed into β form before melting. Observations of isothermal crystal growth rates by optical microscopy revealed that *sn*-PPO β-3L crystals grow faster than the other single TAGs or MCs, particularly above ~18 °C. Differences in the crystallization kinetics between *sn*-PPO, POP, and $MC_{POP/sn\text{-}PPO}$ may cause the separate crystallization while the POP/*sn*-PPO mixture cools.

INTRODUCTION

In many fat-based soft materials, different triacylglycerol (TAG) species demonstrate functional properties such as melting and solidification, structural firmness, viscoelasticity, etc.; these properties cannot be revealed by using a single component.[1] To search the optimal combinations of the TAG species, one must systematically examine the mixing behaviors of different TAGs in binary, ternary, and more complicated mixture systems while in a solid state.[2] First, we must analyze the kinetic and thermodynamic phases of the binary TAG mixtures. Here eutectic, monotectic, solid solution, and molecular compound (MC) forming phases appear differently according to similarity/dissimilarity in the component TAGs' molecular structures.[3-5]

The MC crystals are formed by mixing specific TAG molecules at a certain ratio, typically 1:1.[3] MC-forming TAG mixtures have been reported for various binary mixtures composed of S-U-S, S-S-U, and U-S-U TAGs. S and U represent saturated and unsaturated fatty acid molecules, as summarized in Table 1. In addition to the mechanism by which MC crystals form, the fat mixtures that form MC crystals were examined for edible applications like fatty spreads[12] or confectionery fats.[13]

Despite multiple investigations into the occurrence and physical properties of the MC crystals, the following problems remain unresolved: (1) Why do all the MC crystals form double chain length structures, while the component TAGs form triple chain length structures? (2) Why do MC crystals form in S-U-S/U-S-U (e.g., POP/OPO and SOS/OSO), S-U-S/S-S-U (e.g., POP/PPO and SOS/SSO), U-S-U/U-U-S (e.g., OPO/OOP) mixtures, but not in S-U-S/U-U-S (e.g., POP/OOP[14] and SOS/SOO[15]) and S-S-U/U-S-U (e.g., PPO/OPO[4]) mixtures? (3) What molecular interactions are needed to form MC crystals?

Table 1. MC-forming TAG mixtures

Symmetric/Symmetric (S-U-S/U-S-U)		Symmetric/Asymmetric (S-U-S/S-S-U) (U-S-U/U-U-S)		Asymmetric/Asymmetric (S-S-U/U-U-S)	
SOS/OSO[6]	α-2 β-2	SOS/*rac*-SSO[7,8]	α-2 β'-2 β-2	*rac*-PPO/OOP[4]	sub-α-2 α-2 β'-2
POP/OPO[9]	α-2 β-2	POP/*rac*-PPO[10]	α-2 β'-2 β-2		
PEP/EPE[11]	α-2 β-2	OPO/*rac*-OOP[4]	sub-α-2 β'-2 β-2		

SOS: 1,3-distearoyl-2-oleoyl glycerol, OSO: 1,3-dioleoyl-2-stearoyl glycerol, POP: 1,3-dipalmitoyl-2-oleoyl glycerol, OPO: 1,3-dioleoyl-2-palmitoyl glycerol, PEP: 1,3-dipalmitoyl-2-elaidoyl glycerol, EPE: 1,3-dielaidoyl-2-palmitoyl glycerol, *rac*-SSO: 1,2-distearoyl-3oleoyl-*rac*-glycerol, *rac*-PPO: 1,2-dipalmitoyl-3-oleoyl-*rac*-glycerol, *rac*-OOP: 1,2-dioleoyl-3-palmitoyl-*rac*-glycerol

MC crystals demonstrate complicated crystallization kinetics. For example, Ikeda *et al*. observed that MCs of POP/OPO and POP/PPO can crystallize in neat liquid and diluted solution.[16,17] Nakanishi *et al*. observed that the fast cooling of the 1:1 mixture of POP/OPO caused the separated crystallization of POP and OPO in the metastable forms. In contrast, slow crystallization enabled $MC_{POP/OPO}$ crystal formation and POP and OPO post-crystallization transformation.[18,19] Quite recently, Yoshikawa *et al*. observed in the ternary mixtures of SOS/OSO/LLL (trilauroyl glycerol) that β form crystallization of $MC_{SOS/OSO}$ crystals triggered β crystallization of LLL, which usually crystallizes in the metastable β' form in the absence of

$MC_{SOS/OSO}$.[20] Therefore, unique processes are involved in MC crystals' crystallization kinetics for the TAG mixtures of S-U-S/U-S-U and S-U-S/S-S-U and few past studies have addressed these problems.

In the present study, we observed the crystallization kinetics of polymorphic forms of TAG crystals contained within three mixture: POP/OPO, POP/*rac*-PPO and POP/*sn*-PPO. Here, *sn*-PPO indicates 1,2-dipalmitoyl-3-oleoyl-*sn*-glycerol. We carefully compared the crystallization kinetics of POP/OPO, POP/*rac*-PPO and POP/*sn*-PPO MC crystals to understand the molecular effects on MC crystals formation.

The influences of optical isomerization on the structural and mixing properties of TAGs were systematically studied by Craven and Lencki.[21-23] Mizobe *et al.* examined the polymorphic structures of R-PPO and S-OPP and their mixtures as to two optical isomers of PPO. They found that (1) R-PPO and S-OPP had identical structural properties, (2) the polymorphic structures of the 1:1 mixture of R-PPO/S-OPP and *rac*-PPO were identical, and (3) R-PPO and *rac*-PPO had different polymorphic properties.[24] Therefore, comparing the crystallization kinetics of $MC_{POP/OPO}$, $MC_{POP/rac\text{-}PPO}$, and $MC_{POP/sn\text{-}PPO}$ may elucidate the effects of glycerol structures MC crystal formation.

EXPERIMENTAL SECTION

Materials

Samples of 1,3-dipalmitoyl-2-oleoyl glycerol (POP), 1,3-dipalmitoyl-2-oleoyl glycerol (OPO), and 1,2-dipalmitoyl-2-oleoyl-*rac*-glycerol (*rac*-PPO) (purity ≥ 99%) were purchased from Larodan AB (Solna, Sweden) and used without further purification. Enantiopure 1,2- dipalmitoyl-3-oleoyl-*sn*-glycerol (*sn*-PPO) was provided by Tsukishima Foods Industry Co., Ltd. (Tokyo, Japan), and the sample purity was 99%. Equimolar mixtures of POP/OPO, POP/*rac*-PPO and POP/*sn*-PPO were prepared by combining TAG components at a 1:1 ratio, melted at 50 °C, and homogenized using a vortex mixer.

Differential Scanning Calorimetry

Differential Scanning Calorimetry (DSC) experiments of POP/OPO and POP/*rac*-PPO were conducted at atmospheric pressure by using a PerkinElmer DSC-8000 (Perkin Elmer, Waltham, MA, USA). In contrast, the thermal behavior of samples containing enantiopure *sn*-PPO was analyzed using a Hitachi DSC7000X equipment (Hitachi High-Tech Science Corporation, Tokyo, Japan). The DSC thermograms obtained by the two calorimeters were completely comparable. Samples (4.00-4.60 mg) were weighed into 50 μl aluminum pans and an empty pan was used as a reference. Both instruments were calibrated according to indium's and decane's standard melting temperatures and enthalpies. Dry nitrogen was used as purge gas in the DSC measurement chamber, at a flow rate of 20 cm^3/min in the PerkinElmer DSC-8000 and at 30 cm^3/min in the Hitachi DSC7000X. Thermograms were analyzed using Pyris software to obtain T_{top} and T_{onset} (or T_{end}) transition temperatures. T_{top} corresponded to the temperature at peak-top positions, whereas

T_{onset} (or T_{end}) was defined as the temperature at intersections between baselines and tangents at inflection points of the initial (or final) peak slopes.

The samples were cooled at varied rates of 0.1 °C, 0.5 °C, and 2 °C/min from the melt (50 °C) to complete crystallization (target temperature from 10 °C to -5 °C, depending on the sample and cooling rate applied), then subsequently heated at a constant rate of 2 °C/min.

XRD experiments with laboratory-scale or synchrotron radiation sources were carried out under the same selected thermal treatment to further interpret the DSC thermograms.

Laboratory-scale X-ray diffraction

Laboratory-scale powder X-ray diffraction experiments were performed using two pieces of equipment. POP/OPO and POP/*rac*-PPO samples were analyzed using a PANalytical X' Pert Pro MPD powder diffractometer operating with Debye-Scherrer transmission geometry and equipped with a hybrid monochromator and a PIXcel detector. An Oxford Cryostream Plus 220V (temperature range from 80 K to 500 K) was used for thermal processing of the samples. Samples were introduced in 1 mm-diameter Lindemann glass capillaries, which were rotated around their axis to minimize preferential crystalline orientation. The step size was 0.013° from 1° to 28° of 2θ, and the measuring time was 150 s per pattern.

XRD patterns of samples containing enantiopure *sn*-PPO were obtained by a Rigaku NANO-Viewer with Cu-K_α radiation (40 kV and 30 mA, λ = 0.154 nm) and a two-dimensional detector PILATUS 100K (DECTRIS Ltd. Baden, Switzerland), equipped with a hot stage. Exposure times were 180 s and 15 s for 0.1 °C /min cooling and 2.0 °C /min heating, respectively.

Synchrotron radiation X-ray diffraction

Synchrotron radiation X-ray diffraction (SR-XRD) experiments were carried out using the BL40B2 in the SPring-8 synchrotron radiation facility at the Japan Synchrotron Radiation Research Institute (JASRI) in Hyogo, Japan. The sample was placed into a copper cell with a 10-mm diameter and 0.4-mm thickness. Each cell featured a 3 mm hole covered by Kapton film windows. The energy of the incident X-rays was 12.4 keV (wavelength of 0.1 nm). SR-XRD data were collected using a PILATUS 2M detector (DECTRIS Ltd. Baden, Switzerland) with a camera length of 342.9 mm. Each sample's exposure time was 2 s.

Polarized Optical Microscopy

Polarized optical microscopy (POM) observations were conducted using a Nikon LV 100 microscope (Nikon Co., Tokyo, Japan) with a sensitive color plate under the crossed Nicol condition. Each sample's isothermal crystallization kinetics were recorded using a CMOS camera with EPIX XCAP software. The temperature program was controlled by a LINKAM BCS196 hot stage (Linkam Scientific Instruments Ltd., Tadworth, Surrey, U.K.). All samples were melted at 40 $^{\circ}$C for 2 min and quenched at 60 $^{\circ}$C /min to each isothermal crystallization temperature. The isothermal crystal growth rates of POP, *rac*-PPO, *sn*-PPO, POP/*rac*-PPO, and POP/*sn*-PPO samples were measured in the temperature range from 6 $^{\circ}$C to 28 $^{\circ}$C.

RESULTS and DISCUSSION

All the binary mixtures (at 1:1 ratio) examined were exposed to identical cooling/heating conditions, consisting of cooling from a melted state (50 °C) until complete crystallization at intermediate (2 °C /min) and low rates (0.5 °C and 0.1 °C/min), then subsequently heated at 2 °C/min.

1,3-dipalmitoyl-2-oleoyl glycerol (POP)/1,3-dioleoyl-2-palmitoyl glycerol (OPO)

Figure 1 displays the polymorphic behavior of the POP/OPO mixture at a 1:1 ratio when subjected to cooling and succeeding heating processes at 2 °C/min. When cooled, the DSC cooling curve (Figure 1a) exhibited an exothermic event initiated at 10.4 °C and with a peak top temperature of 3.5 °C. This according to the XRD data (Figure 1b), corresponded to the crystallization of most stable β form of the POP/OPO molecular compound. This form was identified by its double chain length (2L) diffraction peaks of 4.2 and 2.1 nm, and typical β short spacing values of 0.46, 0.45, 0.44, 0.40 and 0.38 nm. The sample simply melted when heated, as shown in the related DSC endothermic signal with the onset and peak top temperatures of 28.8 °C and 31.2 °C, respectively.

As expected, the polymorphic crystallization behavior exhibited by POP/OPO when submitted to lower cooling rates of 0.5 °C and 0.1 °C/min (data not shown) was equivalent to that described above, based on the simple crystallization and melting of the most stable form of $MC_{POP/OPO}$. This agrees with previous work,[25, 26] which confirmed that the reduced cooling rates favor creation of more stable polymorphs.

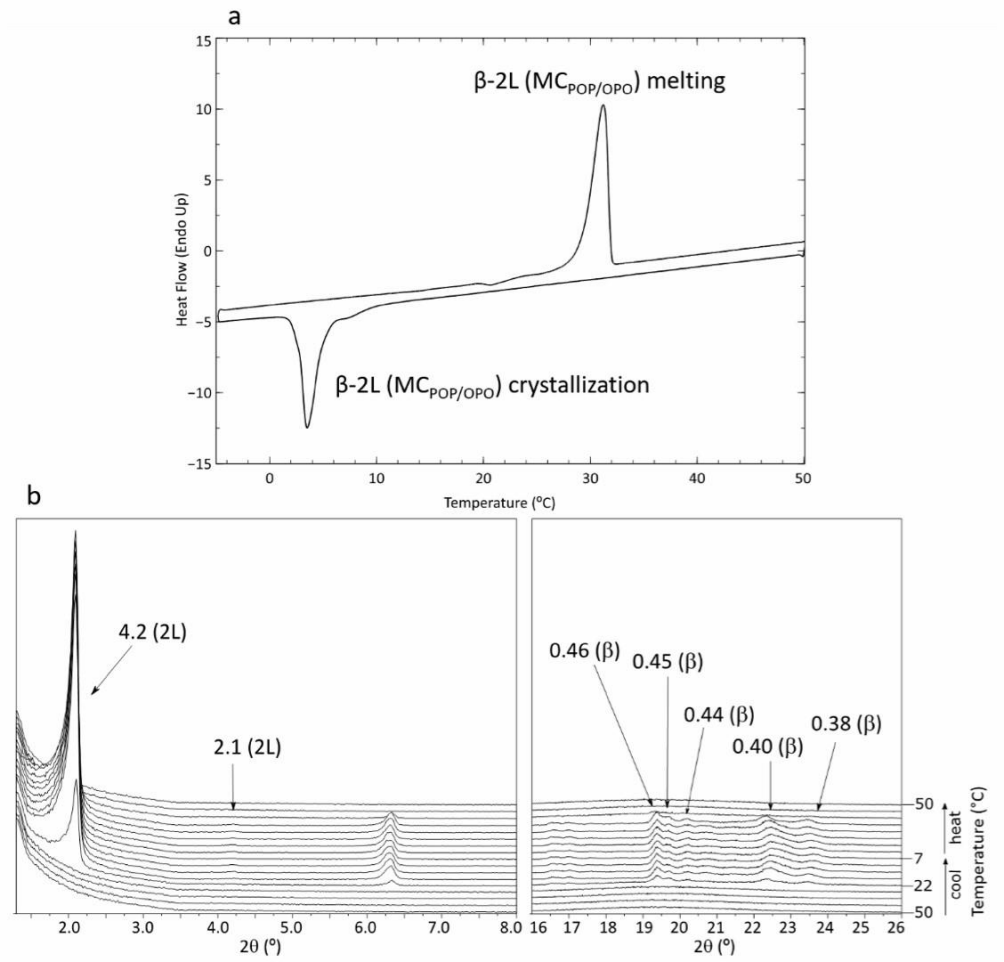

Figure 1. Polymorphic behavior of POP/OPO when cooled and heated at 2 °C/min. (a) DSC thermogram; (b) small- (left) and wide-angle (right) regions of corresponding laboratory-scale XRD patterns. Unit: nm.

1,3-dipalmitoyl-2-oleoyl glycerol (POP)/1,2-dipalmitoyl-3-oleoyl-*rac*-glycerol (*rac*-PPO)

We applied the same experimental conditions to the POP/OPO and POP/*rac*-PPO mixtures. Figure 2 shows selected DSC and XRD results obtained using cooling rates of 0.1 °C and 0.5 °C/min. The polymorphic characteristics displayed by the sample when cooled at 2 °C/min were equivalent to those observed at 0.5 °C/min, so they are omitted here for brevity.

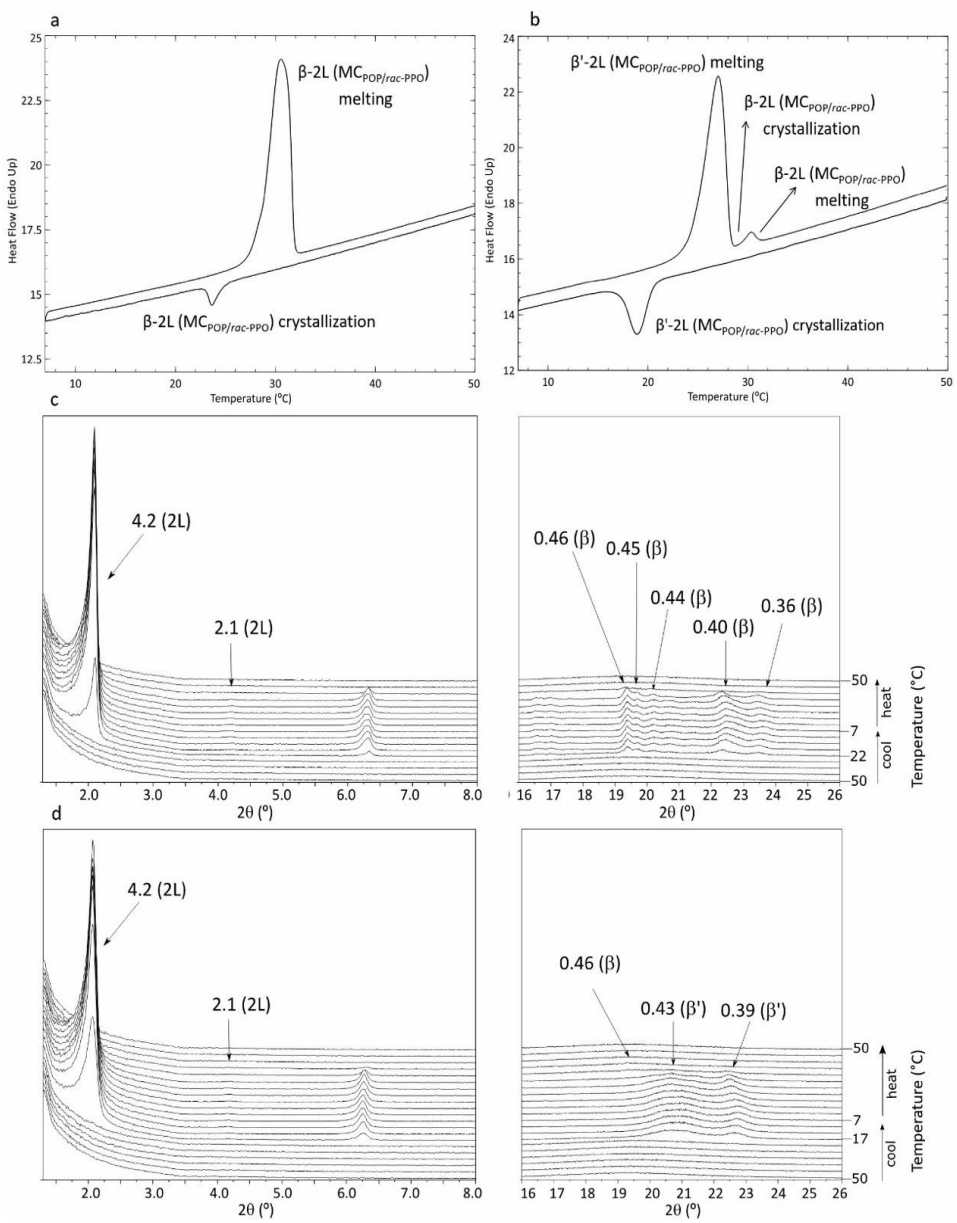

Figure 2. Polymorphic behavior of POP/*rac*-PPO when cooled at 0.1 °C and 0.5 °C/min and heated at 2 °C/min. (a) and (b) DSC thermograms for cooling-heating at 0.1°C–2 °C/min and 0.5 °C–2 °C/min, respectively; (c) and (d) Small- (left) and wide-angle (right) XRD patterns for cooling-heating at 0.1 °C–2 °C/min and 0.5 °C–2 °C/min, respectively.

The polymorphic behavior observed when the POP/*rac*-PPO sample was cooled at 0.1 °C/min and heated at 2 °C/min was equivalent to that of POP/OPO, consisting of the simple

crystallization and melting of the most stable β form of MC$_{POP/rac\text{-}PPO}$ (Figures 2a and 2c). The exothermic DSC signal with onset and peak top temperatures of 25.4 °C and 23.6 °C, respectively, corresponded to the crystallization of β-2L of MC$_{POP/rac\text{-}PPO}$, as XRD was confirmed with the occurrence of reflections with long-spacing values of 4.2 and 2.1 nm, and typical β short spacings of 0.46, 0.45, 0.44, 0.40 and 0.36 nm. When heated, this form melted at 28.1 °C (T_{onset}).

More complicated polymorphic behaviors were observed when the cooling rates were increased to 0.5 °C/min and 2 °C/min, based on the less-stable form development (see Figures 2b and 2d). The β' polymorph of MC$_{POP/rac\text{-}PPO}$, with XRD peaks of 4.2 and 2.1 nm (small-angle region) and 0.43 and 0.39 nm (wide-angle region) crystallized at 20.6 °C (onset DSC temperature). During subsequent heating at 2 °C/min, this form melted (intense endothermic DSC event with an onset temperature of 24.1 °C and peak top temperature of 27.0 °C) and it crystallized into the most stable β form (occurrence of wide-angle region XRD peak of 0.46 nm). However, not all the liquid appeared to have crystallized into β. According to the intensity of corresponding DSC and XRD signals, significantly less of the β form was obtained than the β' form. The last endothermic event, with T_{onset} of 29.1 °C and observable in the DSC heating thermogram, was assigned to the melting of the MC$_{POP/rac\text{-}PPO}$ β phase.

Interestingly, both POP/OPO and POP/*rac*-PPO samples showed MC crystallization and transformation behaviors without separate crystallization of POP, OPO and *rac*-PPO under the experimental conditions examined.

1,3-dipalmitoyl-2-oleoyl glycerol (POP)/1,2-dipalmitoyl-3-oleoyl-*sn*-glycerol (*sn*-PPO)

Mizobe *et al*. observed identical polymorphisms of R-PPO and S-OPP, which crystallized in α-2L with *d*-spacing values of 5.0 nm (cooling), 4.1 nm (heating), and 0.41 nm; and β'-3L with 3.4 nm, 0.42 nm, and 0.39 nm.[24] To confirm this, we subjected isolated *sn*-PPO to a cooling and subsequent heating process at 2 °C/min (see supplementary Figure S1) to identify its polymorphic forms before dealing with its blend with POP. By cooling molten *sn*-PPO at 2 °C /min, SR-XRD data showed β'-3L peaks of 3.4, 0.47, 0.41, and 0.37 nm around 25 °C, associated with a DSC crystallization peak with onset and maximum temperatures of 26.4 °C and 24.8 °C, respectively. Almost simultaneously, an additional weak SR-SAXD α-2L peak of 2.2 nm appeared. When heated, all SR-XRD peaks vanished around 35 °C (melting DSC event with an onset of 35.9 °C and peak top temperature of 37.9 °C). These results are slightly different from those of Mizobe *et al.*,[24] in which β'-3L alone was crystallized by cooling at 2 °C/min, β'-3L and α-2L were concurrently crystallized at 10 °C/min and α-2L alone was crystallized at 50 °C/min. Judging from the relative intensities of the SR-XRD peaks, the quantity of α-2L phase formed may be almost negligible compared to that of β'-3L.

The POP/*sn*-PPO mixture at a 1:1 ratio exhibited significantly intricate polymorphic behavior; unlikely to the mixtures of POP/OPO and POP/*rac*-PPO. Single POP and *sn*-PPO component crystals coexisted with $MC_{POP/sn\text{-}PPO}$ crystals examined under all the thermal treatments applied.

To start with, Figure 3 shows DSC and XRD data obtained when POP/*sn*-PPO was cooled at the lowest rate of 0.1 °C/min and heated at 2 °C/min. Crystallization started at 23.8 °C (initial T_{onset}), manifesting as two exothermic DSC signals with maximum temperatures of 22.8 °C and

21.0 °C. These corresponded to the occurrence of a β'-3L form of single *sn*-PPO, and the concurrent crystallization of $MC_{POP/sn\text{-}PPO}$ β'-2L (and presumably the POP β' form) based on the XRD data.[22] Hence, at about 21 °C, corresponding XRD patterns showed the rise of triple chain length structure peak of 3.5 nm and wide-angle region reflections of 0.42 and 0.38 nm (β'-3L phase of *sn*-PPO) and, at about 17 °C, double chain-length structure signals of 4.2 and 2.2 nm and β' peak of 0.39 nm were discerned (crystallization of β'-2L of $MC_{POP/sn\text{-}PPO}$ and β' form of POP, having identical *d*-spacing values).

When we heated the fully crystallized sample, the XRD peaks of 4.2, 0.42 and 0.39 nm disappeared at 26 °C–27 °C due to the melting of β'-2L forms of $MC_{POP/sn\text{-}PPO}$ and POP. A new small-angle peak of 4.1 and β-type reflection of 0.46 nm were observed at 30 °C. Immediately, the β'-3L form of *sn*-PPO completely melted, as revealed by the total disappearance of the 3.5 nm peak at 31 °C. Then, as only the β form with a double chain length structure was present in the sample's crystalline state in the sample at this temperature, we assume that it corresponded to the most stable β form of $MC_{POP/sn\text{-}PPO}$, which instantly melted at 32 °C. This progressive, but rapid, sequence of polymorphic transformation and melting processes took place along the double endothermic DSC event starting at 24.0 °C (T_{onset}), ending at 34.3 °C (T_{end}). The two peak top temperatures were 26.9 °C and 32.3 °C. The first peak could be assigned to the melting of β' forms of POP and $MC_{POP/sn\text{-}PPO}$, and the second one to the crystallization of β-2L ($MC_{POP/sn\text{-}PPO}$) and melting of the β'-3L (*sn*-PPO) and β ($MC_{POP/sn\text{-}PPO}$) (see Figure 3a).

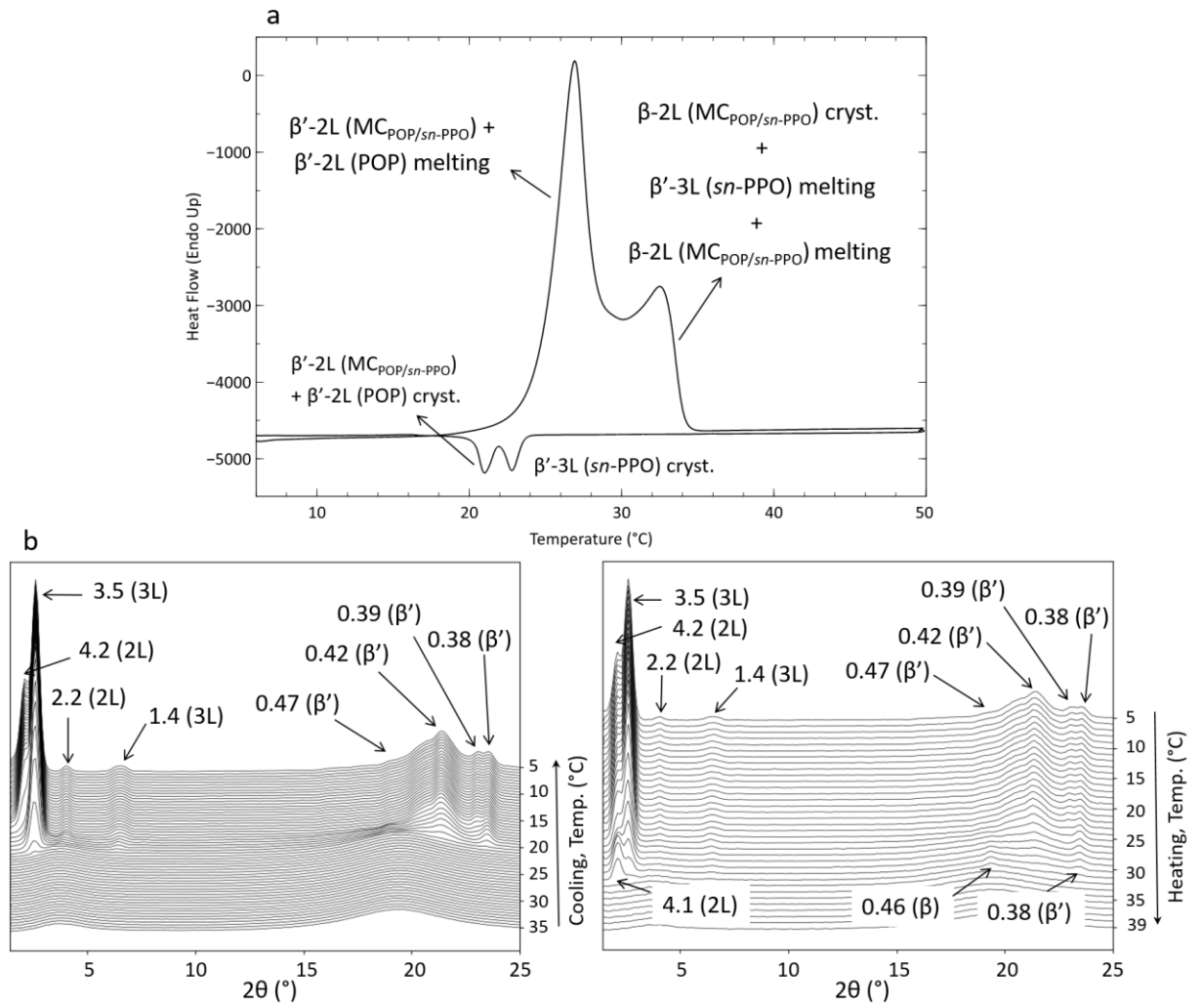

Figure 3. Polymorphic behavior of POP/*sn*-PPO when cooled at 0.1 °C/min and heated at 2 °C/min. (a) DSC thermogram; (b) Laboratory-scale XRD patterns taken during cooling (left) and heating (right). Unit: nm.

Polymorphic behavior of POP/*sn*-PPO when subjected to cooling at 0.5 °C/min and heating at 2 °C/min became equivalent to that of cooling-heating at 0.1 °C/min–2 °C/min, although some differences were detected in the relative intensities of XRD peaks (Figure 4). These will be described later. At 18 °C–19 °C, the *β′*-3L form of the *sn*-PPO component crystallized (3.5, 0.47,

0.41, and 0.38nm), followed by β'-2L forms of $MC_{POP/sn\text{-}PPO}$ and individual POP (small-angle region peaks of 4.2 and 2.2 nm). These crystallization processes were assigned to the double exothermic DSC signal starting at 21.3 °C and with peak top temperatures of 20.3 °C and 17.3 °C. When heated, the lastly formed polymorphs—β'-2L of $MC_{POP/sn\text{-}PPO}$ and POP—melted simultaneously between approximately 22°C–29 °C (first endothermic DSC peak with a top temperature of 26.1°C, Figure 4a). Later, at 30 °C, the most stable β form of $MC_{POP/sn\text{-}PPO}$ crystallized (with 4.1- and 0.46-nm peaks, Figure 4 b). Subsequently, at 31 °C, the 3L peak of 3.5 nm completely vanished due to the melting of β'-3L (*sn*-PPO). At 34 °C, the most stable β-2L form of $MC_{POP/sn\text{-}PPO}$ melted, and no diffraction peaks were present. There was a difference in the relative intensity of the XRD peaks of double-chain length structure, 2L (4.2 nm, corresponding to β' forms of $MC_{POP/sn\text{-}PPO}$ and POP) to those of triple-chain length structure, 3L (3.5 nm, assigned to β' polymorph of *sn*-PPO), when comparing the cooling rates of 0.1 °C/min (Figure 3b) and 0.5 °C/min (Figure 3b). We assume that lower cooling rates may favor the formation of the MC crystals, as molecules may have more time to arrange themselves. Thus, the increased intensity of the 2L peak of 4.2 nm observed when cooled at 0.5 °C/min may be due to higher amounts of β' POP formation, rather than MC. Additionally, much lower amounts of β $MC_{POP/sn\text{-}PPO}$ were discerned during heating after cooling at 0.5 °C/min than after cooling at the lowest rate of 0.1 °C/min. This was confirmed by observing the lower intensities of the 4.1 and 0.46 nm characteristic peaks in the former case (see Figures 3b and 4b).

The crystallization and transformation behaviors of the POP/*sn*-PPO mixture became more complex when the cooling rate was increased because metastable forms emerged for both $MC_{POP/sn\text{-}PPO}$ and single TAG components. Figure 5 shows the DSC and related SR-XRD patterns

obtained when the POP/*sn*-PPO sample was subjected to a cooling and subsequent heating processes at an intermediate rate of 2 °C/min.

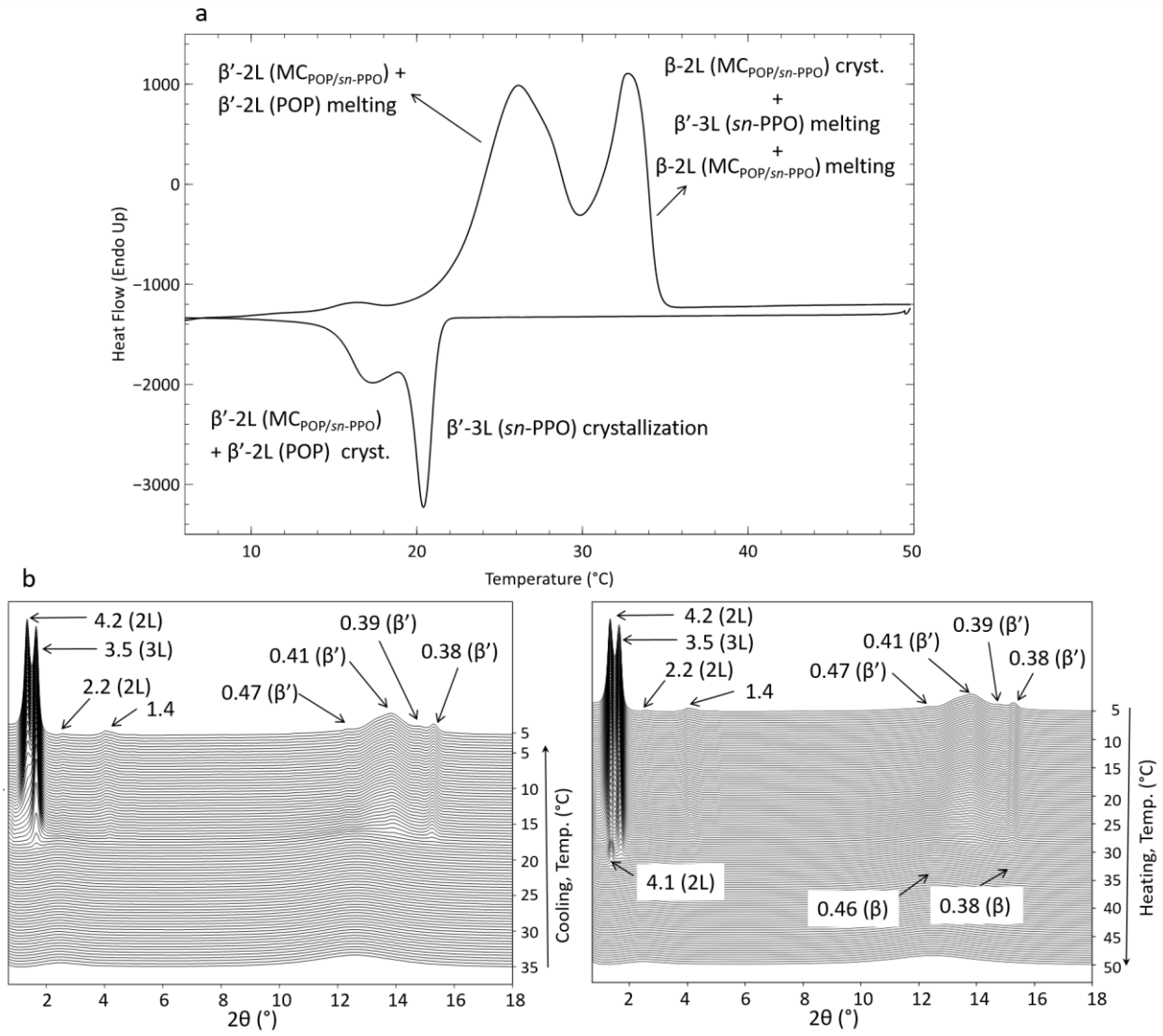

Figure 4: Polymorphic behavior of POP/*sn*-PPO when cooled at 0.5 °C/min and heated at 2 °C/min. (a) DSC thermogram; (b) Laboratory-scale XRD patterns taken during cooling (left) and heating (right). Unit: nm.

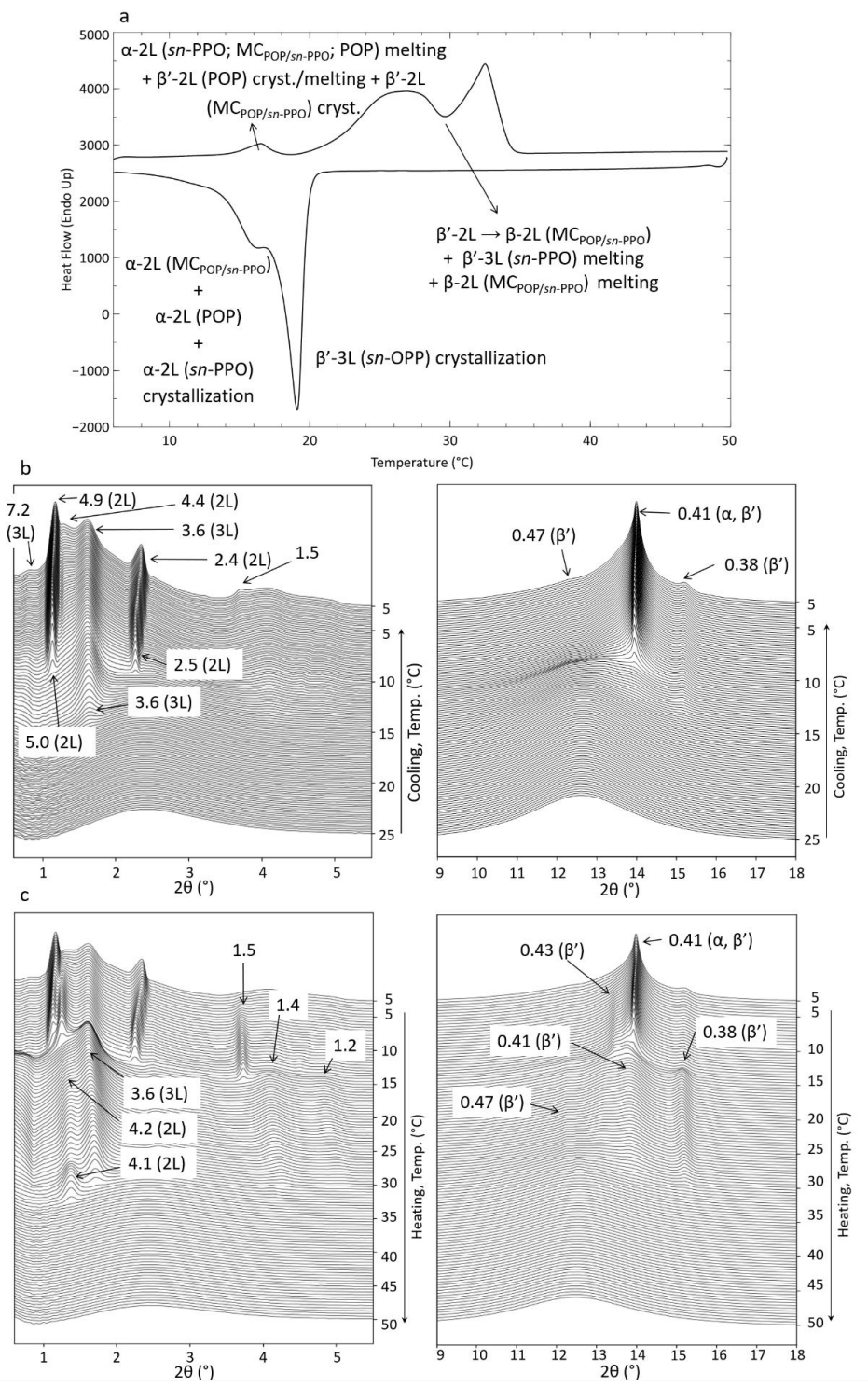

Figure 5. Polymorphic behavior of POP/*sn*-PPO when cooled and heated at 2 °C/min. (a) DSC thermogram; (b) SR-SAXD (left) and SR-WAXD (right) patterns taken during cooling; (c) SR-SAXD (left) and SR-WAXD (right) patterns taken during heating. Unit: nm.

When cooled after melting, triple chain-length SR-SAXD peaks at 7.2 and 3.6 nm, accompanied by SR-WAXD reflections of 0.41 and 0.38 nm—typical of β'-3L (*sn*-PPO)—appeared at about 15 °C. Then, at 11 °C, new 2L SR-SAXD peaks of 5.0 (which shifted to 4.9 during cooling) and 2.5 nm occurred. Simultaneously, the α peak intensity of 0.41 nm increased. These changes could have been caused by the crystallization of the least stable α-2L of $MC_{POP/sn\text{-}PPO}$, which could coexist with the α-2L form of POP individual TAG.[24] By cooling close to 8 °C, a very weak diffraction signal of 4.4 nm was assigned to the development of α-2L (*sn*-PPO). This was previously identified by its 002 reflections of 2.2 nm (Figure S1). These sequenced crystallization phenomena appeared in the DSC cooling thermogram as an exothermic event starting at 20.1 °C and having two peak top temperatures of 19.1 °C and 16.0 °C (see Figure 5a).

When the crystallized sample was heated, the SR-SAXD weak peak of 4.4 nm increased in intensity, and a new SR-WAXD β'-type signal of 0.43 nm appeared. Meanwhile, the 4.9 nm peak fully disappeared at 14 °C and that of 0.41 nm peak was meaningfully decreased in intensity. This could be interpreted as the melting of all previously formed least stable α-2L polymorphs of *sn*-PPO, $MC_{POP/sn\text{-}PPO}$, and POP and the succeeding crystallization of a β'-2L form, probably of POP, which melted at 16 °C (fading of the 4.4 nm reflection). At 17 °C, the intensity of the 3L peak at 3.6 nm started to diminish immediately. At 4.2 nm, it became sharper, most likely because of the β'-2L form of $MC_{POP/sn\text{-}PPO}$. These melting and transformation processes were related to the broad endothermic DSC peak with a maximum temperature of 16.5 °C. Upon further heating (at about 29 °C), the β'-2L form of $MC_{POP/sn\text{-}PPO}$ transformed into its most stable β-2L form. This was identified through the shifting of the 4.2 nm peak to 4.1 nm and subsequent increase in intensity. Then, β'-3L (*sn*-PPO) and β-2L ($MC_{POP/sn\text{-}PPO}$) melted at 32 °C and 33 °C, respectively, and no more diffraction peaks were observed at higher temperatures. The polymorphic transformation from β'

to β $MC_{POP/sn\text{-}PPO}$ and melting of β'-3L (*sn*-PPO) and β-2L ($MC_{POP/sn\text{-}PPO}$) were associated with the broad endothermic DSC signal with top temperatures of 26.7 °C and 32.5 °C. However, all these complex transformations and melting processes may be considered as a continuous phenomenon taking place during all the heating treatments. However, the assignment of thermal events to single polymorphic events process is hindered by the multiple metastable forms with similar *d*-spacing values and by broad DSC signals.

Comparison of MC crystals of POP/OPO, POP/*rac*-PPO and POP/*sn*-PPO polymorphisms

Figure 6 summarizes the crystallization and transformation pathways exhibited by POP/OPO, POP/*rac*-PPO and POP/*sn*-PPO when subjected to cooling procedures at 0.1 °C, 0.5 °C and 2 °C /min and subsequent heating at 2 °C /min.

The POP/OPO mixture solely formed the most stable β-2L form of $MC_{POP/OPO}$ at all the experimental conditions examined, even when the intermediate cooling rate of 2 °C/min was applied. The occurrence of MC in the β polymorph was already reported in the n-dodecane solution system at different concentrations[16] and in the melt.[9] However, the metastable α form was also obtained at a higher cooling rate of 15 °C/min. In any case, the 1:1 ratio mixture of POP and OPO solely formed MC. We detected no coexistence with any pure TAG components during any of the experiments.

In contrast, β' and β polymorphs were formed in the $MC_{POP/rac\text{-}PPO}$ crystals. The most stable β form crystallized at the lowest cooling rate of 0.1 °C/min, whereas higher rates of 0.5 °C and 2 °C/min led to polymorphic crystallization resulting in the less-stable β' phase, which was

transformed into a stable β during heating. Again, crystallizations of POP and *rac*-PPO were not observed in these conditions, as previous work by Minato *et al*. also confirmed. [10]

The POP/*sn*-PPO mixture manifested a significantly complicated crystallization behavior, as demonstrated by multiple polymorphic forms of $MC_{POP/sn\text{-}PPO}$, and each of the single TAG components of POP and *sn*-PPO. The most stable β'-3L form of *sn*-PPO appeared almost simultaneously with β'-2L forms of $MC_{POP/sn\text{-}PPO}$ and POP when cooled at 0.1 °C and 0.5 °C/min. When heated, the most stable β-2L form of $MC_{POP/sn\text{-}PPO}$ was obtained from its β'-2L form through the melt-mediation process. These crystallization processes became more complex when the cooling rate was increased to 2 °C/min. Here, the least stable α forms predominated during crystallization, transforming into more stable phases when heated. In more detail, we obtained the β'-3L (*sn*-PPO) form, followed by the α forms of $MC_{POP/sn\text{-}PPO}$, POP, and *sn*-PPO. Then, α-2L polymorphs of POP and $MC_{POP/sn\text{-}PPO}$ were transformed into their respective β' forms during heating. $MC_{POP/sn\text{-}PPO}$ proceeded with its polymorphic transformation until it achieved its most stable β form.

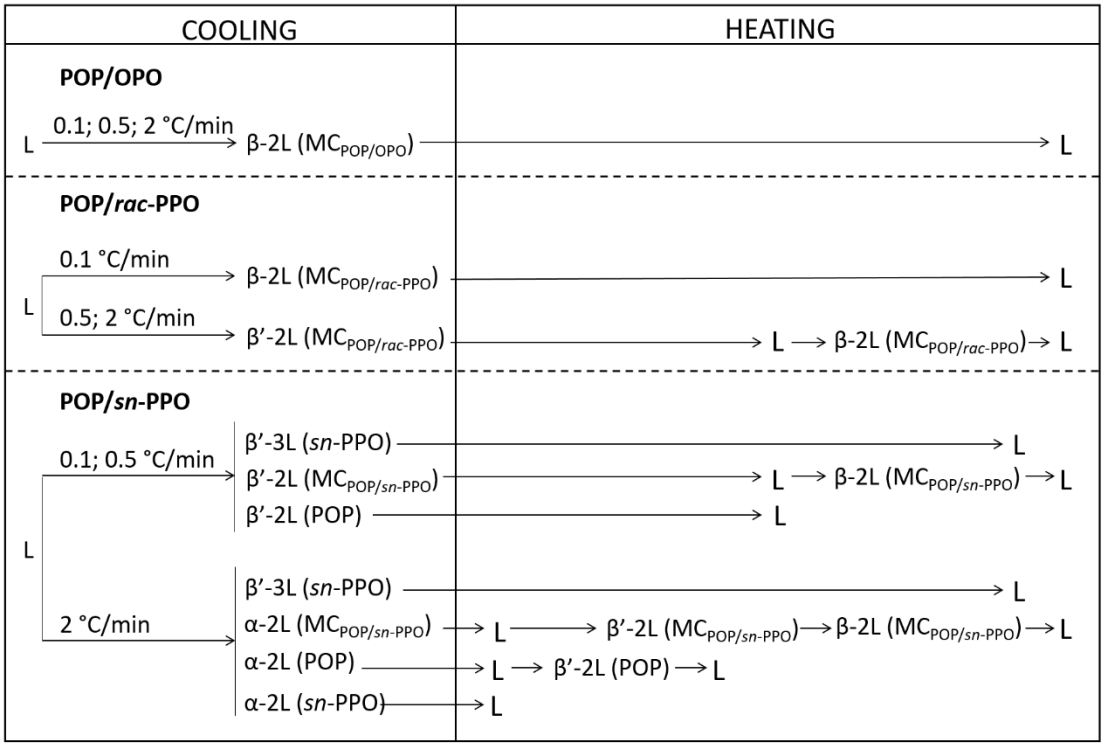

Figure 6. Polymorphic crystallization and transformation pathways of POP/OPO, POP/*rac*-PPO and POP/*sn*-PPO samples at varying cooling rate conditions (0.1 ˚C, 0.5 ˚C, and 2 ˚C/min). All heating processes occurred at 2 ˚C/min.

POM observations and growth rates

POM observations were conducted to examine each sample's growth kinetics and clarify the reason why single TAG components grew in the POP/*sn*-PPO mixture before $MC_{POP/sn\text{-}PPO}$ crystals grew during cooling.

Figure 7 shows examples of the POM images during isothermal growth: *rac*-PPO at 16 ˚C (Figure 7 (a)), and *sn*-PPO, POP, $MC_{POP/rac\text{-}PPO}$, and $MC_{POP/sn\text{-}PPO}$ at 20 ˚C (Figure 7 (b)(f)). *rac*-PPO and *sn*-PPO crystallized into typical β' form spherulites above 18 ˚C and into worm-like crystallites of α form[24] below 18 ˚C. POP, $MC_{POP/rac\text{-}PPO}$, and $MC_{POP/sn\text{-}PPO}$ formed worm-like α

form crystals similar to *rac*-PPO below 14 °C. POP formed spherulites of γ-3L form between 14 °C to 20 °C; and $MC_{POP/rac\text{-}PPO}$ and $MC_{POP/sn\text{-}PPO}$ formed those of β' form above 14 °C.

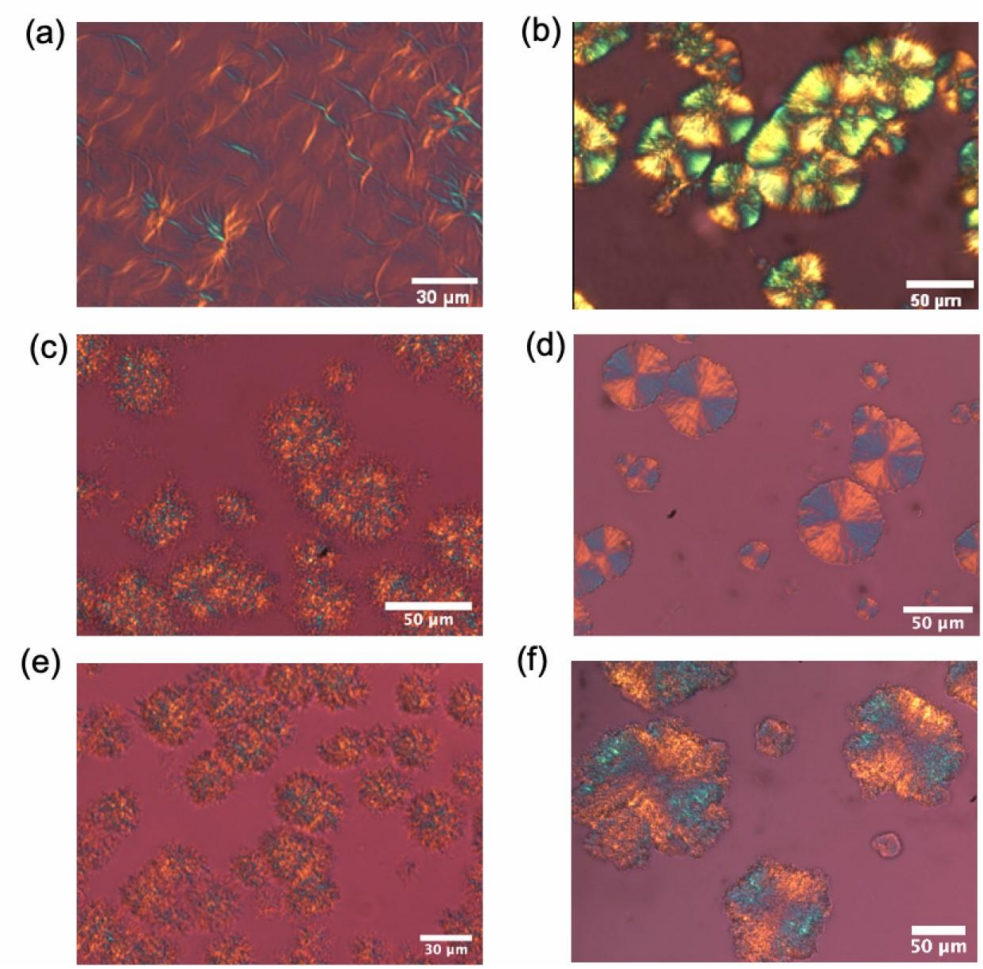

Figure 7. POM images during isothermal growth of (a) *rac*-PPO α form at 16 °C, and at 20 °C of (b) POP, (c) *rac*-PPO, (d) *sn*-PPO, (e) POP/*rac*-PPO, and (f) POP/*sn*-PPO.

The isothermal growth rates, V, of each of the worm-like α crystallites and spherulites were determined by measuring the time evolution of the growing tips or the size of spherulites.[27] The temperature dependencies of the crystal growth rates for the TAG samples are shown in Figure 8. Above 18 °C, the growth rate of *sn*-PPO crystals (β'-3L) was significantly higher (by almost two

orders of magnitude) than the others. In the lower temperature range, the growth rates of α form of POP grew more slowly than the others.

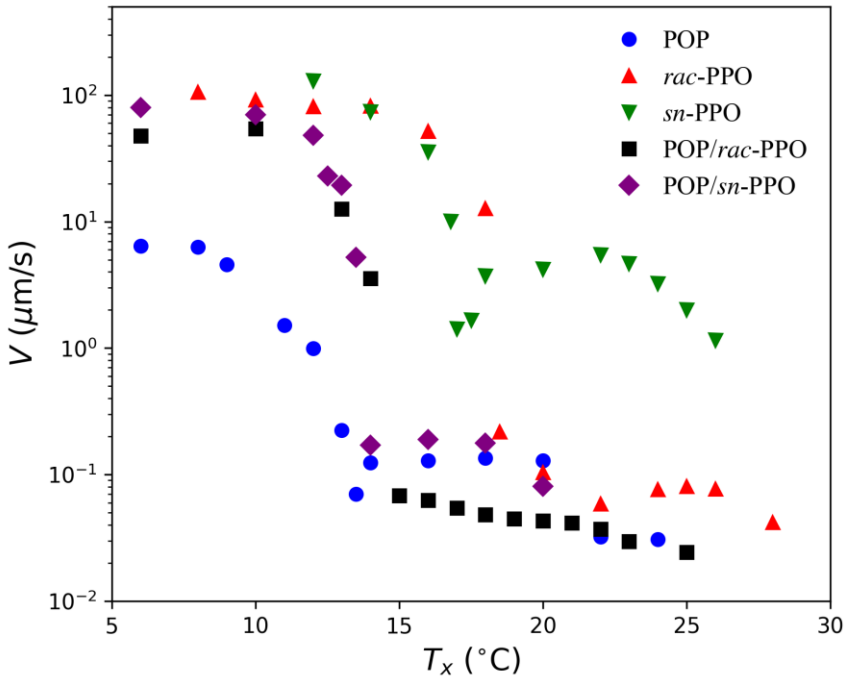

Figure 8. Temperature dependence of the crystal growth rates, V, of POP, *rac*-PPO, *sn*-PPO, $MC_{POP/rac\text{-}PPO}$, and $MC_{POP/sn\text{-}PPO}$. T_x represents the isothermal crystallization temperature. The growth rates were measured for worm-like α forms at low temperatures below 18 °C (*rac*-PPO and *sn*-PPO) and 14 °C (POP and MCs), and for spherulitic γ (POP) and β' (the others) forms at higher temperatures.

Differences in growth rates between *sn*-PPO and POP and $MC_{POP/sn\text{-}PPO}$ were much greater than those between *rac*-PPO and POP and $MC_{POP/sn\text{-}PPO}$. This extremely large difference in the growth rate between *sn*-PPO, POP and $MC_{POP/sn\text{-}PPO}$ could cause the growth of the *sn*-PPO β'-3L form before the $MC_{POP/sn\text{-}PPO}$ and POP β'-2L form when the POP/*sn*-PPO 1:1 mixture is cooled, as

shown in Figure 6. As the cooling rate increased, the crystallization temperature of *sn*-PPO *β′*-3L decreased and approached that of the growth rate maximum. It would result in the increase of the relative concentration of *sn*-PPO crystals (*β′*-3L) at higher cooling rates. This phenomenon was observed in the first DSC exothermic peak during cooling processes as shown in Figures 3–5. With increasing cooling rates, higher amounts of *sn*-PPO crystallized at lower temperatures. The remaining POP and *sn*-PPO could suppress the melt state to within the temperature range where the *α* form grew, as shown in Figures 5 and 6. These were obtained at a cooling rate of 2 ◦ ◦C/min.

Effects of glycerol conformations on crystallization kinetics of MC

Differences in the crystallization behavior for $MC_{POP/OPO}$ and $MC_{POP/sn\text{-}PPO}$ can be discussed by comparing the glycerol structures of POP, OPO, and *sn*-PPO and the structure models of $MC_{POP/OPO}$ and $MC_{POP/sn\text{-}PPO}$, as show in Figure 9. As for *β* of POP, we can assume a tuning fork-type glycerol conformation, in which two palmitic acid chains connected to the *sn*-1 and *sn*-3 glycerol carbon atoms (hereafter referred to as *sn*-1,3-palmitic) faced upward in this figure. In contrast, the one oleic acid chain connected to the *sn*-2 glycerol carbon atom (*sn*-2 oleic) faces the opposite direction. A single-crystal X-ray diffraction experiment confirmed the tuning fork conformation in *β*-form of tricaproyl-glycerol.[28] The same glycerol conformation can be applied to *β* of OPO, in which oleic and palmitic acid chains of POP are replaced with palmitic and oleic acid chains, respectively. In both TAGs, the triple chain length structure forms on the stable *β* polymorph so that the palmitic and oleic acid chains are stacked at the different leaflets. This avoids the steric hindrance between straight palmitic chains and bent oleic acid chains.

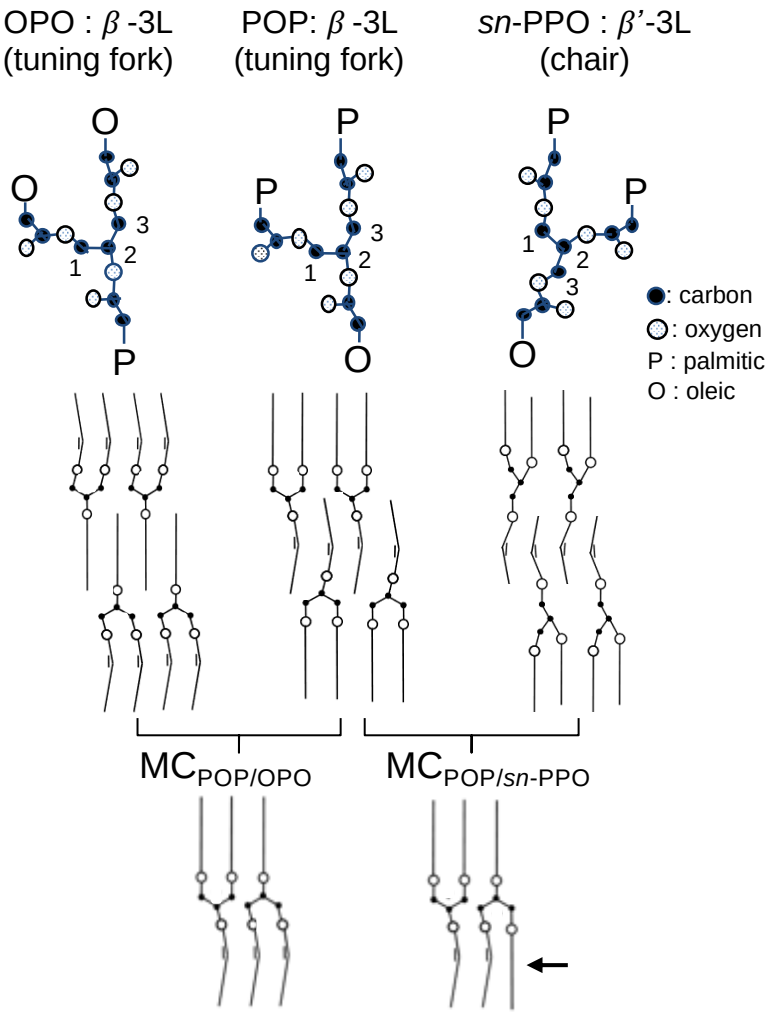

Figure 9. Glycerol conformations, chain length stacking and molecular compound (MC) crystals made of POP, OPO and *sn*-PPO

In contrast, *β'* of *sn*-PPO may demonstrate a chair-type glycerol conformation, which was observed in *β'* polymorph of 1,2-dipalmitoyl-3-myristoyl-*sn*-glycerol by single-crystal X-ray diffraction experiment.[29] In *β'* of *sn*-PPO, sn-1,2 palmitic acid chains face up, whereas the *sn*-3 oleic acid chain is faces down. If we define this *sn*-PPO as R-PPO, S-OPP must consist of *sn*-1 oleic acid chain and *sn*-2,3 palmitic acid chains. In both *β'* forms of R-PPO and S-OPP, the triple chain length structure is formed for the same reasons as those for POP and OPO.

MC crystal formation within the 1:1 mixtures of POP/OPO and POP/*sn*-PPO requires the component TAGs to undergo two rearrangements. Firstly, the chain length structure should change from triple of POP, OPO and *sn*-PPO to double of the MC crystals. Secondly, close packing of glycerol groups and palmitic and oleic acid chains between the neighboring TAGs should be formed. $MC_{POP/sn\text{-}PPO}$ formation is more difficult than that of $MC_{POP/OPO}$, because (1) excess kinetic processes are necessary to arrange the chair-type glycerols of *sn*-POP and the tuning fork-type POP for $MC_{POP/sn\text{-}PPO}$, whereas such rearrangement processes are unnecessary for $MC_{POP/OPO}$, and (2) the palmitic and oleic chains are separately stacked in different lamellae in $MC_{POP/OPO.}$ In contrast, the palmitic and oleic chains are stacked in the same lamellae of $MC_{POP/sn\text{-}PPO}$ as shown by an arrow in Figure 9. Therefore, the crystallization rates of $MC_{POP/sn\text{-}PPO}$ are lowered, and the crystallization of pure TAGs of POP and *sn*-PPO exceeds over that of $MC_{POP/sn\text{-}PPO}$ with increasing rates of cooling, as summarized in Figure 6.

The crystallization behaviors of $MC_{POP/rac\text{-}PPO}$ and $MC_{POP/sn\text{-}PPO}$ are different. While the origins of these differences are not easily explained, but two optical isomers of R-PPO and S-OPP likely form stable molecular packing. This allows MC crystals to form in cooperation with the two POP molecules. The molecular mechanisms of $MC_{POP/OPO}$, $MC_{POP/rac\text{-}PPO}$, and $MC_{POP/sn\text{-}PPO}$ formations and transformations should be addressed by future studies.

CONCLUSIONS

We compared the polymorphic crystallization and transformation behaviors of three MC-forming 1:1 binary TAG mixture systems during cooling and heating: POP/OPO, POP/*rac*-PPO, and POP/*sn*-PPO. The POP/OPO mixture showed simple crystallization and melting of the $MC_{POP/sn\text{-}OPO}$ β-2L form. The POP/*rac*-PPO mixture also crystallized into the β-2L form of

$MC_{POP/rac\text{-}PPO}$ for the low cooling rates of 0.1 °C/min, but into the less-stable *β′*-2L form at higher cooling rates of 0.5 °C and 2 °C/min. Only the MCs have formed in both POP/OPO and POP/*rac*-PPO mixtures, whereas every single component crystallized separately in the POP/*sn*-PPO mixture. In the POP/*sn*-PPO mixture, *sn*-PPO *β′*-3L crystallized at first while cooling, followed by the formation of POP and $MC_{POP/sn\text{-}PPO}$ *β*′-2L for the slow cooling of 0.1 and 0.5 °C/min; *α*-2L was formed during fast cooling of 2 °C/min. The isothermal crystal growth rates determined by optical microscopy revealed that *sn*-PPO *β*-3L crystals grow significantly faster than the other single TAG components (POP and *rac*-PPO) and MCs ($MC_{POP/rac\text{-}PPO}$ and $MC_{POP/sn\text{-}PPO}$), particularly above ~18 °C. This large difference in growth kinetics could cause the separate crystallization of processes to occur for each component during cooling. MC formation can be affected by individual component's growth kinetics; hence, MC formation might depend on the cooling rate, particularly for the TAG mixtures containing optical isomer components. Further studies are needed to understand the molecular mechanisms capable of altering crystallization kinetics.

ASSOCIATED CONTENT

Supporting Information

The Supporting Information is available free of charge.

Figure-S1: DSC and SR-XRD results for *sn*-PPO when cooled and heated at 2 °C/min in (PDF).

AUTHOR INFORMATION

Corresponding Author

Ken Taguchi − Graduate School of Advanced Science and Engineering, Hiroshima University, Higashi-Hiroshima 739-8521, Japan; orcid.org/ 0000-0003-1276-0499; Phone: +81-82-424-6538; Email: ktaguchi@hiroshima-u.ac.jp

Authors

Laura Bayés-García – Departament de Mineralogia, Petrologia i Geologia Aplicada, Universitat de Barcelona, Barcelona, Spain

Koji Fukao – Department of Physics, Ritsumeikan University, Kusatsu, Shiga 525-8577, Japan

Takashi Konishi – Graduate School of Human and Environmental Studies, Kyoto University, Sakyo-ku, Kyoto 606-8501, Japan

Kiyotaka Sato – Faculty of Applied Biological Science, Hiroshima University, Higashi-Hiroshima 739-8528, Japan

Author Contributions

Conceptualization: L.B.G., K.T., and K.S.; methodology: L.B.G., K.F., T.K., and K.T.; validation: L.B.G., K.T., and K.S.; formal analysis: L.B.G. and K.T.; investigation: L.B.G. and K.T.; data curation: L.B.G. and K.T.; writing, original draft preparation: L.B.G., K.T., and K.S.; writing, review and editing: L.B.G., K.T., and K.S.; visualization: L.B.G., K.T, and K.S.; supervision: K.S.; project administration: L.B.G. and K.T.; funding acquisition: L.B.G. and K.T. All authors read and agreed to the published version of the manuscript.

Notes

The authors have no competing financial interests to declare.

ACKNOWLEDGEMENTS

The authors acknowledge the financial support of Grant PID2019-107032RB-I00 funded by MCIN/AEI/10.13039/501100011033/. This work was also supported by JSPS KAKENHI Grant Number JP16K05405. The synchrotron radiation experiments were performed at the BL40B2 of SPring-8 with the approval of the Japan Synchrotron Radiation Research Institute (JASRI) (Proposal Nos. 2020A1078, 2020A1111, 2020A1348, 2021B1190 and 2022B1548). We appreciate Dr. N. Ohta in the Diffraction and Scattering Division of JASRI for his special assistance with SR-XRD measurements.

ABBREVIATION

DSC, differential scanning calorimetry; XRD, X-ray diffraction; SR-XRD, Synchrotron radiation X-ray diffraction; POP, 1,3-dipalmitoyl-2-oleoyl glycerol; OPO, 1,3-dioleoyl-2-palmitoyl glycerol; *rac*-PPO, 1,2-dipalmitoyl-3-oleoyl-*rac*-glycerol; *sn*-PPO, 1-oleoyl-2,3-dipalmitoyl-*sn*-glycerol

REFERENCES

(1) Marangoni, A. G.; Wesdorp, L. H. Structure and properties of fat crystal networks, 2nd ed.; CRC Press, 2013.

(2) Floeter, E.; Haeupler, M.; Sato, K. Molecular interactions and mixing phase behavior of lipid crystals. Crystallization of Lipids. Fundamentals and Applications in Food, Cosmetics and Pharmaceuticals; Sato, K., Ed 2018, 61–104.

(3) Macridachis-González, J.; Bayés-García, L.; Calvet, T. An insight into the solid-state miscibility of triacylglycerol crystals. Molecules 2020, 25, 4562–4589.

(4) Bayés-García, L.; Calvet, T.; Cuevas-Diarte, M. À.; Ueno, S.; Sato, K. Phase Behavior of Binary Mixture Systems of Saturated-Unsaturated Mixed-Acid Triacylglycerols: Effects of Glycerol Structures and Chain–Chain Interactions. The Journal of Physical Chemistry B 2015, 119, 4417–4427.

(5) Zhang, L.; Ueno, S.; Sato, K. Binary phase behavior of saturated-unsaturated mixedacid triacylglycerols—A review. Journal of Oleo Science 2018, ess17263.

(6) Koyano, T.; Hachiya, I.; Sato, K. Phase behavior of mixed systems of SOS and OSO. The Journal of Physical Chemistry 1992, 96, 10514–10520.

(7) Engström, L. Triglyceride Systems Forming Molecular Compounds. Lipid / Fett 1992, 94, 173–181.

(8) Takeuchi, M.; Ueno, S.; Sato, K. Crystallization kinetics of polymorphic forms of a molecular compound constructed by SOS (1,3-distearoyl-2-oleoyl-sn-glycerol) and SSO (1,2-distearoyl-3-oleoyl-rac-glycerol). Food research international 2002, 35, 919–926.

(9) Minato, A.; Ueno, S.; Yano, J.; Smith, K.; Seto, H.; Amemiya, Y.; Sato, K. Thermal and structural properties of sn-1,3-dipalmitoyl-oleoylglycerol and sn-1,3-dioleoyl-2palmitoylglycerol binary mixtures examined with synchrotron radiation X-ray diffraction. J. Am. Oil Chem. Soc. 1997, 74, 1213–1220.

(10) Minato, A.; Ueno, S.; Smith, K.; Amemiya, Y.; Sato, K. Thermodynamic and Kinetic Study on Phase Behavior of Binary Mixtures of POP and PPO Forming Molecular Compound Systems. J. Phys. Chem. B 1997, 101, 3498–3505.

(11) Zhang, L.; Wei, K. J.; Chen, J. C.; Xiong, M.; Li, X.; Hondoh, H.; Ueno, S. Effect of cis–trans isomerization on the crystallization behavior of triacylglycerols. Crystal Growth & Design 2020, 20, 1655–1664.

(12) Sibbald, A.; Carney, J.; Marangoni, A. Enhanced structuring of fat with reduced saturates using mixed molecular compounds. Journal of the American Oil Chemists' Society 2016, 93, 1441–1452.

(13) Watanabe, S.; Yoshikawa, S.; Sato, K. Formation and properties of dark chocolate prepared using fat mixtures of cocoa butter and symmetric/asymmetric stearic-oleic mixed-acid triacylglycerols: Impact of molecular compound crystals. Food Chemistry 2021, 339, 127808.

(14) Zhang, L.; Ueno, S.; Miura, S.; Sato, K. Binary phase behavior of 1,3-dipalmitoyl-2-oleoyl-sn-glycerol and 1,2-dioleoyl-3-palmitoyl-rac-glycerol. Journal of the American Oil Chemists' Society 2007, 84, 219–227.

(15) Zhang, L.; Ueno, S.; Sato, K.; Adlof, R.; List, G. Thermal and structural properties of binary mixtures of 1,3-distearoyl-2-oleoyl-glycerol (SOS) and 1,2-dioleoyl-3-stearoylsn-glycerol (sn-OOS). Journal of thermal analysis and calorimetry 2009, 98, 105–111.

(16) Ikeda, E.; Ueno, S.; Miyamoto, R.; Sato, K. Phase behavior of a binary mixture of 1,3dipalmitoyl-2-oleoyl-sn-glycerol and 1,3-dioleoyl-2-palmitoyl-sn-glycerol in n-dodecane solution. The Journal of Physical Chemistry B 2010, 114, 10961–10969.

(17) Ikeda-Naito, E.; Hondoh, H.; Ueno, S.; Sato, K. Mixing phase behavior of 1,3-dipalmitoyl-2-oleoyl-sn-glycerol (POP) and 1,2-dipalmitoyl-3-oleoyl-rac-glycerol (PPO) in n-dodecane solution. Journal of the American Oil Chemists' Society 2014, 91, 1837–1848.

(18) Nakanishi, K.; Mikiya, Y.; Ishiguro, T.; Ueno, S. Crystallization Behavior of Molecular Compound in Binary Mixture System of 1,3-Dioleoyl-2-Palmitoyl-sn-Glycerol and 1,3-Dipalmitoyl-2-Oleoyl-sn-Glycero. Journal of the American Oil Chemists' Society 2018, 95, 51–59.

(19) Nakanishi, K.; Ueno, S. Mixing Ratio and Cooling Rate Dependence of Molecular Compound Formation in OPO/POP Binary Mixture. Molecules 2020, 25.

(20) Yoshikawa, S.; Watanabe, S.; Yamamoto, Y.; Kaneko, F.; Sato, K. Interactive Polymorphic Crystallization Behavior in Eutectic Triacylglycerol Mixtures Containing Molecular Compound Crystals. Crystal Growth & Design 2022, 22, 1753–1763.

(21) Craven, R. J.; Lencki, R. W. Crystallization, Polymorphism, and Binary Phase Behavior of Model Enantiopure and Racemic Triacylglycerols. Cryst. Growth Des., 2011, 11, 1723-1732.

(22) Craven, R. J.; Lencki, R. W. Symmetry, Chirality and Crystalline Tendency: the Polymorphism of triacylglycerols. Food Funct. 2012, 3, 228-233.

(23) Craven, R. J.; Lencki, R. W. Polymorphism of Acylglycerols: A Stereochemical Perspective. Chem. Rev., 2013, 113, 7402-7420.

(24) Mizobe, H.; Tanaka, T.; Hatakeyama, N.; Nagai, T.; Ichioka, K.; Hondoh, H.; Ueno, S.; Sato, K. Structures and Binary Mixing Characteristics of Enantiomers of 1-Oleoyl-2,3-dipalmitoyl-sn-glycerol (S-OPP) and 1,2-Dipalmitoyl-3-oleoyl-sn-glycerol (R-PPO). Journal of the Americal Oil Chemists' Society 2013, 90, 1809–1817.

(25) Bayés-García, L.; Calvet, T.; Cuevas-Diarte, U. S., Miquel Àngel; Sato, K. In situ observation of transformation pathways of polymorphic forms of 1,3-dipalmitoyl-2-oleoyl glycerol (POP) examined with synchrotron radiation X-ray diffraction and DSC. CrystEngComm 2013, 15, 302–314.

(26) Bayés-García, L.; Calvet, T.; Cuevas-Diarte, M.; Ueno, S. In situ crystallization and transformation kinetics of polymorphic forms of saturated-unsaturated-unsaturated triacylglycerols: 1-palmitoyl-2,3-dioleoyl glycerol, 1-stearoyl-2,3-dioleoyl glycerol, and 1palmitoyl-2-oleoyl-3-linoleoyl glycerol. Food Research International 2016, 85, 244–258.

(27) Taguchi, K.; Toda, A.; Hondoh, H.; Ueno, S.; Sato, K. Kinetic Study on Alpha-Form Crystallization of Mixed-Acid Triacylglycerols POP, PPO, and Their Mixture. Molecules 2021, 26, 220.

(28) Jensen, L. H.; Mabis, A. J. Refinement of the Structure of β-Tricaprin. Acta Cryst. 1966, 22, 770-781.

(29) Sato, K.; Goto, M.; Yano, J.; Honda, K.; Kodali, D. R.; Small, D. M. Atomic Resolution Structure Analysis of β' polymorph crystal of a triacylglycerol: 1,2-dipalmitoyl-3-myristoyl-*sn*-glycerol. J. Lipid. Res., 2001, 42, 338-345.